

Possible quantum spin liquid state of CeTa₇O₁₉

N. Li,^{1,*} A. Rutherford,^{2,*} Y. Y. Wang,¹ H. Liang,¹ Y. Zhou,¹ Y. Sun,¹ D. D. Wu,¹ P. F. Chen,¹ Q. J. Li,³ H. Wang,⁴ W. Xie,⁴ E. S. Choi,⁵ S. Z. Zhang,⁶ M. Lee,⁶ H. D. Zhou,^{2,†} and X. F. Sun^{1,‡}

¹Anhui Provincial Key Laboratory of Magnetic Functional Materials and Devices,
Institutes of Physical Science and Information Technology,
Anhui University, Hefei, Anhui 230601, People's Republic of China

²Department of Physics and Astronomy, University of Tennessee, Knoxville, Tennessee 37996, USA

³School of Physics and Optoelectronics, Anhui University,
Hefei, Anhui 230061, People's Republic of China

⁴Department of Chemistry, Michigan State University, East Lansing, Michigan 48824, USA

⁵National High Magnetic Field Laboratory, Florida State University, Tallahassee, FL 32310, USA

⁶Los Alamos National Laboratory, Los Alamos, New Mexico 87545, USA

(Dated: March 6, 2025)

CeTa₇O₁₉ is a recently found two-dimensional triangular lattice antiferromagnet without showing magnetic order. We grew high-quality CeTa₇O₁₉ single crystals and studied the low-temperature magnetic susceptibility, specific heat and thermal conductivity. The dc magnetic susceptibility and magnetization reveal its nature of effective spin-1/2, easy axis anisotropy, and antiferromagnetic spin coupling. The ultralow-temperature ac susceptibility and specific heat data indicate the absence of any phase transition down to 20 mK. The ultralow-temperature thermal conductivity (κ) at zero magnetic field exhibits a non-zero residual term $\kappa_0/T = 0.0056$ W/K²m. Although the magnetic field dependence of κ is rather weak, the 14 T thermal conductivity shows an essential zero residual term. All these results point to a possible ground state of quantum spin liquid.

I. INTRODUCTION

Two-dimensional (2D) triangular lattice antiferromagnet (TAF) with spin-1/2 is the simplest geometrically frustrated system with strong quantum spin fluctuations, which can exhibit exotic quantum magnetisms including the celebrated quantum spin liquid (QSL) [1–4]. Actually, Anderson first proposed the resonating valence bond (RVB) model to describe this novel quantum disorder state based on Heisenberg TAFs [5]. In real materials, the organic TAFs κ -(BEDTTF)₂Cu₂(CN)₃ and EtMe₃Sb[Pd(dmit)₂]₂ with $S = 1/2$ are the early identified QSL candidates [6, 7]. For inorganic materials, some QSL candidates have also been found in TAFs, including YbMgGaO₄, *ARCh*₂ ($A =$ alkali or monovalent ions, $R =$ rare earth ions, $Ch =$ chalcogenides), Na₂BaCo(PO₄)₂, PrMAl₁₁O₁₉ ($M =$ Zn, Mg), Ba₆R₂Ti₄O₁₇ ($R =$ rare earth ions), YbZn₂GaO₅, NaRuO₂, and TbInO₃ etc. [8–16] However, the inevitable disorder effects such as vacancies, impurities, lattice distortion, and stacking faults in real materials induce serious difficulties in accurately characterizing the real ground state in theory and experiments. For example, there is a site mixing between nonmagnetic Mg²⁺ and Ga³⁺ ions in YbMgGaO₄, causing the controversy on the ground state and the low-energy magnetic excitations [17–19].

NdT₇O₁₉ was recently proposed as a rare QSL candidate with Ising anisotropy [20], based on the magneti-

zation, electron spin resonance and muon spin relaxation results. This material has a hexagonal crystal structure with the space group $P\bar{6}c2$. In this compound, the Nd³⁺ ions with effective 1/2-spin form a 2D triangular lattice without structural disorder. Later, Wang *et al.* synthesized various RTa₇O₁₉ ($R =$ Pr, Sm, Eu, Gd, Dy, Ho) which all do not order at low temperatures down to 2 K [21]. Very recently, another two sister materials CeTa₇O₁₉ and YbTa₇O₁₉ were also synthesized and found to have possible QSL ground state [22]. CeTa₇O₁₉ is also a Ising-like TAF with very weak exchange interaction (~ 0.22 K), while YbTa₇O₁₉ has an in-plane magnetic anisotropy. It is notable that all these previous studies demonstrated that RTa₇O₁₉ have perfect triangular spin lattice and would be a good platform to probe the possible QSL in TAFs. Till now, the single crystal samples are not available for most members of this family, which prevents more characterizations on the nature of ground states.

Three experimental hallmarks have been widely accepted as evidence for the QSL state and the associated spinon excitations, including a broad continuous magnetic intensity in the inelastic neutron scattering spectrum [17, 23], a large magnetic specific heat with power-law temperature dependence [24, 25], and a non-zero residual thermal conductivity κ_0/T at zero-Kelvin limit [7, 26–28]. In this work, we grew high-quality CeTa₇O₁₉ single crystal and studied its magnetic ground state by using the ultralow-temperature thermal conductivity, as well as the magnetic susceptibility and specific heat measurements. Besides the absence of magnetic order transition indicated by the ultralow-temperature ac susceptibility and specific heat, a non-zero κ_0/T was observed. These results suggest a possible QSL ground state of

* These authors contributed equally to this work.

† hzhou10@utk.edu

‡ xfsun@ahu.edu.cn

CeTa₇O₁₉.

II. EXPERIMENTS

CeTa₇O₁₉ single crystals were grown by using the flux method. The mixture of CeO₂, Ta₂O₅, and V₂O₅ with molar ratio 0.25:0.1:0.65 was loaded in a Pt crucible with cover. The mixture was annealed at 1200 °C for 40 hours and then cooled down to 900 °C with 0.5 °C/hour rate, and thereafter was cooled to room temperature by air quench. The flux was dissolved in hot HCl acid and crystals with plate shape were recovered. The Laue back diffraction measurement was used to determine the crystalline orientation. The single crystal X-ray diffraction (SCXRD) measurement was performed using a XtalLAB Synergy, Dualflex, Hypix single crystal X-ray diffractometer with Mo K_α radiation ($\lambda = 0.71073$ Å). The structure was solved and refined using the Bruker SHELXTL Software Package.

The dc magnetic susceptibility between 2 and 300 K were measured using the SQUID-VSM (Quantum Design Magnetic Property Measurement System, MPMS) in magnetic field up to 7 T. The ac susceptibility was measured using the conventional mutual inductance technique (with a combination of ac current source and a lockin amplifier) at SCM1 dilution fridge magnet of the National High Magnetic Field Laboratory, Tallahassee. The high field magnetization was measured in the pulsed field facility at Los Alamos National Laboratory by detecting the field-induced voltage across a pick-up coil made of high purity Cu. The specific heat was measured by relaxation technique using the Physical Property Measurement System (PPMS) (DynaCool, Quantum Design) with a dilution insert. The thermal conductivity was measured by using “one heater, two thermometers” technique in a dilution refrigerator equipped with a 14 T magnet [26, 27, 29]. The heat current was along the longest direction (*a* axis) and the external magnetic fields were applied along the *a* axis or the *c* axis.

III. RESULTS AND DISCUSSIONS

The refinement of the SCXRD data confirms that CeTa₇O₁₉ is isostructural to NdTa₇O₁₉ with Ce³⁺ ions forming the 2D triangular lattice, as shown in Figs. 1(a) and 1(b). The refinement results are listed in Table I and II. Our CeTa₇O₁₉ single crystals are brown colored with typical size of 2–3 mm, as shown in the inset to Fig. 1(d). The good crystallinity was confirmed by the X-ray back reflection Laue photograph, as shown in Fig. 1(c). Furthermore, Fig. 1(d) shows the X-ray diffraction pattern of single crystals, which was found to be the (00*l*) diffraction. No impurity phase was detected. The X-ray rocking curve of the (006) peak is very narrow (the full width of the half maximum is only 0.0073°), which also indicates the good crystallinity.

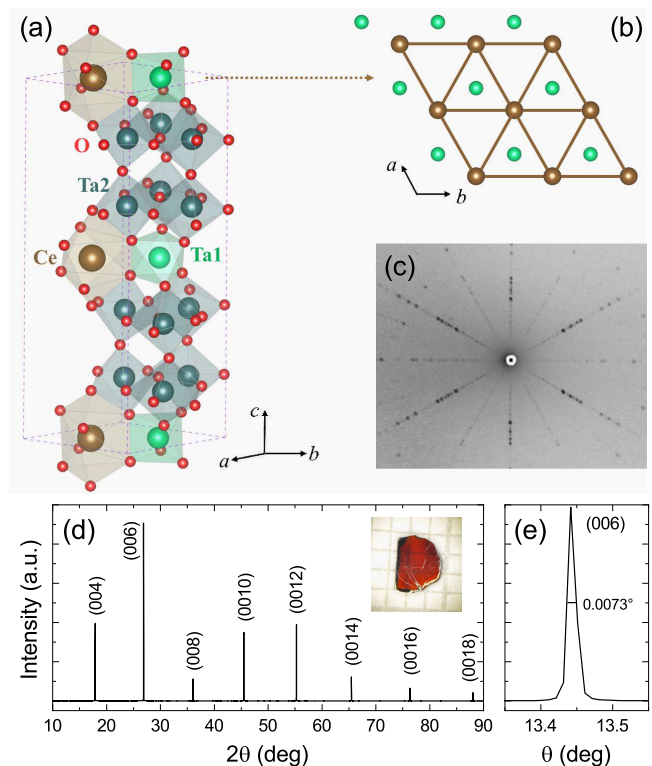


FIG. 1. (a,b) The schematic crystal structure of CeTa₇O₁₉, where Ce³⁺ ions form into an ideal triangular layer in the *ab* plane and these triangular layers are stacked along the *c* axis with the nearest-neighbor interlayer distance of 9.9915 Å. (c) The X-ray Laue back diffraction photo for the *ab* plane. (d,e) X-ray diffraction pattern of (00*l*) plane and the rocking curve of the (006) peak. The full width at the half maximum (FWHM) of the rocking curve is shown in panel (e). The inset to panel (d) shows the photograph of CeTa₇O₁₉ single crystal.

Figures 2(a) and 2(c) present the temperature dependence of magnetic susceptibility χ measured in $B = 0.1$ T along the *c* and *a* axis, respectively. The $\chi(T)$ increases upon lowering temperature and no visible anomaly can be observed down to 2 K, indicating the absence of long-range magnetic order. In addition, the zero-field-cooling (ZFC) and field-cooling (FC) data are identical, which indicates there is no spin freezing. The temperature dependence of χ does not follow Curie-Weiss law well in the whole temperature range, although the high-temperature and low-temperature data can be separately fitted. The Curie-Weiss fit to the low-temperature data gives $\mu_{eff} = 1.755 \mu_B$, $\theta_{CW} = -0.469$ K for $B \parallel c$ and $\mu_{eff} = 1.169 \mu_B$, $\theta_{CW} = -1.383$ K for $B \parallel a$, respectively. These results indicate the dominant antiferromagnetic interactions. Figures 2(b) and 2(d) show the isothermal magnetization curves at selected temperatures with the external magnetic fields along the *c* and *a* axis, respectively. The data clearly suggest easy axis anisotropy since the magnetization reaches around $0.8 \mu_B$ at $B = 7$ T for $B \parallel c$, but only $0.35 \mu_B$ at $B = 7$ T for $B \parallel a$.

TABLE I. The crystal structure and refinement for CeTa₇O₁₉ at room temperature (Mo K α radiation). Values in parentheses are estimated standard deviation from refinement.

Chemical Formula	CeTa ₇ O ₁₉	
Formula weight	1710.77 g/mol	
Space Group	$P - 6c2$	
Unit cell dimensions	$a = 6.2371(2) \text{ \AA}$ $c = 19.9830(7) \text{ \AA}$	
Volume	$673.23(4) \text{ \AA}^3$	
Z	2	
Density(calculated)	8.439 g/cm ³	
Absorption coefficient	60.043 mm ⁻¹	
F(000)	1442.0	
2θ range	7.544 to 82.132°	
Reflections collected	8108	
Independent reflections	1489 [$R_{\text{int}} = 0.0888$]	
Refinement method	Full-matrix least-squares on F ²	
Data/restraints/parameters	1489 / 0 / 45	
Final R indices	$R_1 (I > 2\sigma(I)) = 0.0341$; $wR_2 (I > 2\sigma(I)) = 0.0763$ $R_1(\text{all}) = 0.0385$; $wR_2(\text{all}) = 0.0789$	
Largest diff. peak and hole	+4.01 e/ \AA^3 and -3.08 e/ \AA^3	
R.M.S. deviation from mean	0.955 e/ \AA^3	
Goodness-of-fit on F ²	1.046	

TABLE II. Atomic coordinates and equivalent isotropic atomic displacement parameters (\AA^2) of CeTa₇O₁₉. (U_{eq} is defined as one third of the trace of the orthogonalized U_{ij} tensor.)

CeTa ₇ O ₁₉	Wyck.	x	y	z	Occ.	U_{eq}
Ta ₁	2a	0	0	0	1	0.006(2)
Ta ₂	12l	0.02593(2)	0.33193(12)	0.15613(2)	1	0.007(1)
Ce ₁	2c	1/3	2/3	0	1	0.008(1)
O ₁	12l	0.42017(19)	0.33583(20)	0.15360(3)	1	0.013(1)
O ₂	6k	0.08257(18)	0.37653(20)	1/4	1	0.010(2)
O ₃	12l	0.04227(12)	0.27983(12)	0.05690(3)	1	0.009(1)
O ₄	4g	0	0	0.16830(6)	1	0.007(2)
O ₅	4h	1/3	2/3	0.13250(7)	1	0.009(2)

The recent crystal electric field (CEF) studies [22] on polycrystalline CeTa₇O₁₉ samples reveal that (i) the first excited CEF doublet lies at a very large energy gap 42.9 meV above the ground state and therefore, at low temperature, the ground state of Ce³⁺ ions could be treated as effective spin-1/2; (ii) the powder averaged saturation is around 0.82 μ_B and $\mu_{eff} = 1.42 \mu_B$; (iii) the system is Ising like. All these observations are consistent with our magnetic properties listed above for crystalline samples.

Figure 3(a) shows the ultralow-temperature ac magnetic susceptibility of CeTa₇O₁₉ single crystal measured at zero dc field. The data show that there is no magnetic transition at low temperatures down to 20 mK. Figure 3(b) shows the high-field magnetization curves with the magnetic field along the a axis. At 1.6 K, after a linear subtraction by considering the Van Vleck paramagnetic contribution, the system saturates around 15 T with saturation moment $\sim 0.8 \mu_B$. This again confirms the easy axis nature of CeTa₇O₁₉ since along the c axis, the system reaches 0.8 μ_B at much lower field around 7 T. Moreover, we measured the magnetic field dependence of ac susceptibility at ultralow temperatures for $B \parallel a$ and $B \parallel c$ to

detect the possible field-induced transitions. As shown in Figs. 3(c) and 3(d), there is no any field-induced transition up to 0.5 T. Apparently, the magnetization behavior is quite simple in CeTa₇O₁₉, which is different from some other QSL candidates with triangular lattice [26, 27, 30].

Figure 4 shows the specific heat of CeTa₇O₁₉ single crystal under various magnetic fields. Clearly, there is no phase transition at low temperatures down to 70 mK, which demonstrates the disordered ground state of this material. At very low temperatures, the zero-field data show strong upturn which is likely due to the Schottky contribution of Ce³⁺. With applying magnetic field along the c axis, a broad peak shows up and moves to higher temperatures, which is also a typical Schottky behavior.

It can be seen that the magnetic contributions to the specific heat are significant only at very low temperatures. We can fit the phonon specific heat for the zero-field data at $T > 2$ K. It is known that in the temperature range $0.02 < T/\Theta_D < 0.1$ (Θ_D is the Debye temperature), one can use the low-frequency expansion of the Debye function, $C = \beta T^3 + \beta_5 T^5 + \beta_7 T^7$, where β , β_5 and β_7 are temperature-independent coefficients [31].

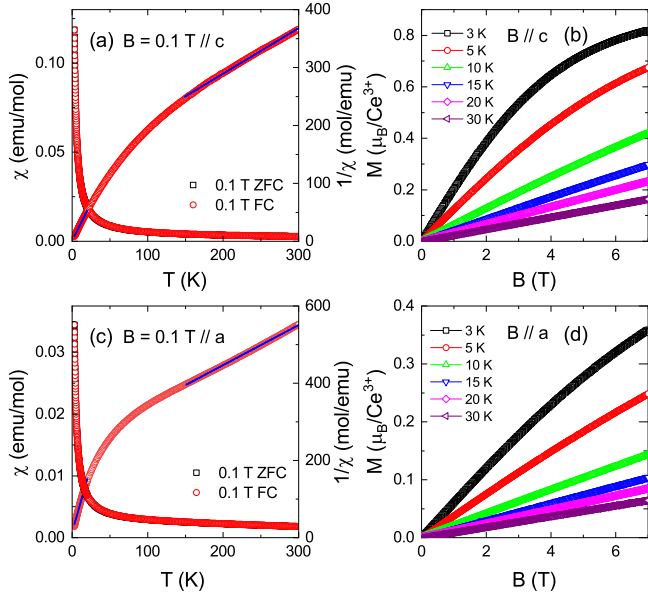


FIG. 2. Temperature dependence of magnetic susceptibility χ and inverse magnetic susceptibility $1/\chi$ of $\text{CeTa}_7\text{O}_{19}$ single crystals with $B \parallel c$ (a) or $B \parallel a$ (c). The solid blue lines indicate the linear fit of the inverse magnetic susceptibility $1/\chi(T)$ curves. Isothermal magnetization of $\text{CeTa}_7\text{O}_{19}$ single crystals at selected temperatures with $B \parallel c$ (b) or $B \parallel a$ (d).

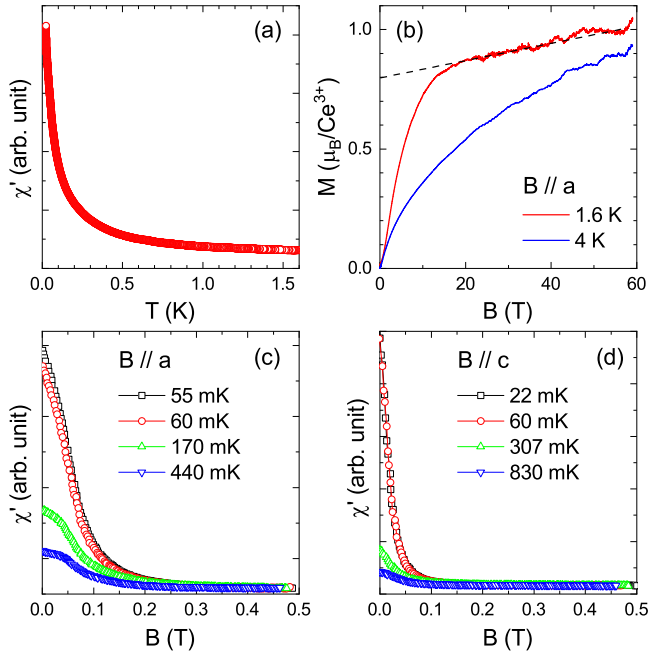


FIG. 3. (a) Ultralow-temperature ac magnetic susceptibility of $\text{CeTa}_7\text{O}_{19}$ single crystal with frequency 220 Hz and 0.5 Oe ac field. (b) High-field magnetization curves with the magnetic field along the a axis. The dashed line shows the Van Vleck paramagnetic term. (c, d) The field dependence of ac susceptibility at different temperatures for $B \parallel a$ and $B \parallel c$.

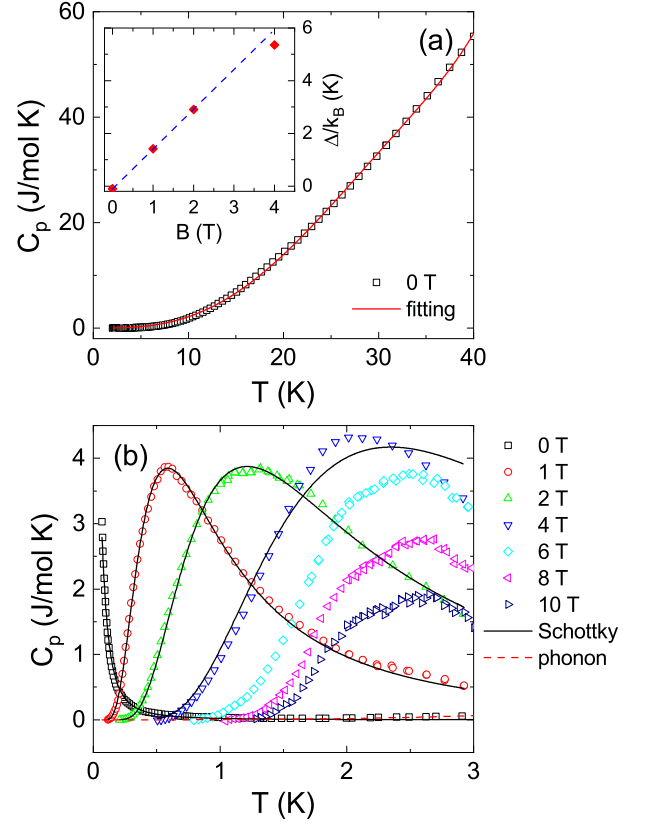


FIG. 4. (a) Zero-field specific heat of $\text{CeTa}_7\text{O}_{19}$ single crystal at 2–40 K. The solid line is the fitting result of high-temperature phononic specific heat. (b) Ultralow-temperature (down to 70 mK) specific heat under different magnetic fields with $B \parallel c$. The dashed line shows the phonon term and the solid lines show the fittings of the Schottky term. The inset shows the fitting parameter Δ in the two-level Schottky formula.

As shown in Fig. 4(a), this formula gives a good fitting to the experimental data, with the fitting parameters $\beta = 2.30 \times 10^{-3} \text{ J/K}^4\text{mol}$, $\beta_5 = -1.56 \times 10^{-6} \text{ J/K}^6\text{mol}$ and $\beta_7 = 4.20 \times 10^{-10} \text{ J/K}^8\text{mol}$. At very low temperatures, the T^5 - and T^7 - terms are negligible and the phonon specific heat shows a well-known T^3 dependence with the coefficient of β . As shown in Fig. 4(b), the phonon specific heat is much smaller than the experimental data at $T < 2$ K. Thus, the very low temperature specific heat under various fields are dominantly the magnetic contributions. We further use the two-level Schottky formula to fit these data,

$$C_{sch} = nR \left(\frac{\Delta}{k_B T} \right)^2 \frac{e^{\Delta/k_B T}}{[1 + e^{\Delta/k_B T}]^2}, \quad (1)$$

where n is the concentration of Schottky centers, R is the universal gas constant, k_B is the Boltzmann constant, and Δ is the gap of the Zeeman splitting of the Kramers doublet ground state of Ce^{3+} ions [31]. As shown in Fig. 4(b), the fitting are quite good for low-field data

but fails at high magnetic fields. The fitting parameter Δ increases linearly with magnetic field up to 2 T, in consistent with the Zeeman effect. That is, this energy gap is the splitting of the ground-state doublet of Ce^{3+} crystal field levels. However, the Δ starts to deviate from linearity at 4 T. Furthermore, above 6 T, the position of peak does not change with increasing magnetic field. It is notable that the behavior of present magnetic specific heat is not common in other Ce^{3+} compounds or QSL candidates. The magnetic specific heat of those materials often exhibits broad peak even in zero field and the peak gradually shifts to higher temperature with increasing magnetic field. Usually, this peak is described as the onset of coherent quantum fluctuations or spin correlations instead of the Schottky anomaly [32–35]. In some cases, the data showed that orphan magnetic moments trapped in defects or the crystal-field excitations of rare-earth ions cause a Schottky-like anomaly and one can also use the simple two-level Schottky model to fit such kind of data [36–41]. For a comparison, the QSL candidate $\text{Ce}_2\text{Zr}_2\text{O}_7$ has a broad peak of magnetic specific heat in zero field, which shifts to higher temperature with increasing the external magnetic field [32]. The two-level Schottky model fitting parameter Δ also starts to deviate from linear field dependence at 4 T in $\text{Ce}_2\text{Zr}_2\text{O}_7$. Based on this analysis, the authors of this work actually ruled out the case that the existence of defects causes the broad peak of magnetic specific heat. Applying magnetic field to QSL candidates can sometimes induce phase transitions, which can be probed by the field dependence of specific heat, as seen in YbMgGaO_4 and NaYbCh_2 [26, 30]. However, for $\text{CeTa}_7\text{O}_{19}$ the values of specific heat are very small at $B > 6$ T and $T < 1$ K, making it difficult to detect the possible phase transitions from the specific heat data.

Figure 5(a) shows the low-temperature thermal conductivity of the $\text{CeTa}_7\text{O}_{19}$ single crystal in 0 T and 14 T with $B \parallel c$. As one can see, the 14 T thermal conductivity is smaller than that in zero field at ultralow temperatures and is slightly larger at high temperatures. That is, the external magnetic field has rather weak effect on the thermal conductivity. We further analyzed the data at very low temperatures, as shown in Fig. 5(b). The $\kappa(T)$ curve does not show the standard T^3 behavior of phonon thermal conductivity at very low temperatures. This indicates that either heat carriers other than phonons or some peculiar phonon scattering effect are involved, since at subKelvin temperatures the common phonon scatterings by crystal imperfections are smeared out [47, 48]. Actually, as shown in Fig. 5(b), the lowest-temperature data show a good linear behavior in the κ/T vs T^α plot. Using the formula $\kappa/T = a + bT^{1.5}$ to fit the data at $T < 200$ mK, we get the residual term a or $\kappa_0/T = 0.0056$ W/K²m for the zero-field data. Here, the two terms represent contributions from the itinerant fermionic excitations and phonons, respectively. With applying 14 T magnetic field along the c axis, the data also show a linear behavior in the κ/T vs $T^{1.4}$ plot at very

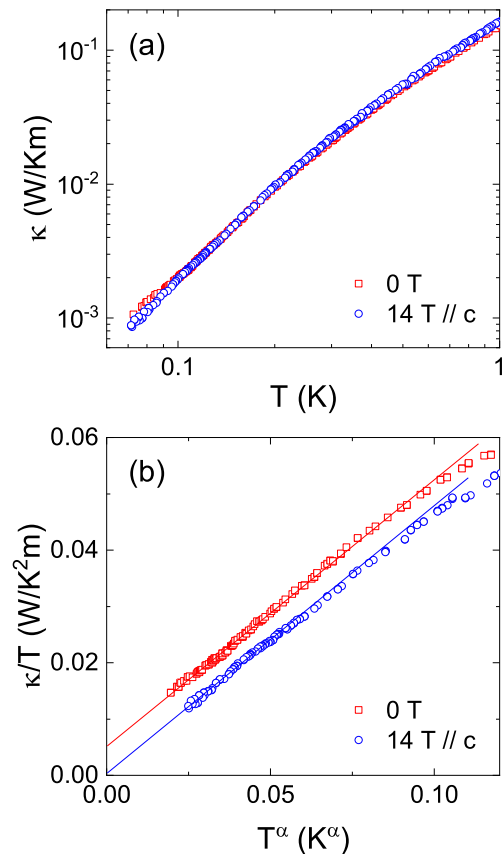


FIG. 5. (a) Low-temperature thermal conductivity of the $\text{CeTa}_7\text{O}_{19}$ single crystal in zero field and 14 T along the c axis. (b) Ultralow-temperature data plotted with κ/T vs T^α ($\alpha = 1.5$ and 1.4 for 0 T and 14 T, respectively). The solid lines are the linear fittings to the data.

low temperatures and the linear fitting gives an essential zero residual term, which is in the expectation that high magnetic field suppresses the fermionic excitations.

The non-zero κ_0/T term at zero-Kelvin limit is often considered one of key evidences for a QSL ground state and has been extensively studied in recent years. However, the residual thermal conductivity remains a topic of debate in certain QSL candidates, such as $\text{EtMe}_3\text{Sb}[\text{Pd}(\text{dmit})_2]_2$, YbMgGaO_4 , and $1T\text{-TaS}_2$ and is mainly related to the influence of unavoidable disorders [7, 26, 28, 42–45]. In this work, the κ_0/T in zero field is in the same order of magnitude with those of some quantum magnets having itinerant fermionic excitations [26, 27, 29]. The above thermal conductivity results indicate that in zero field there are likely itinerant spinons. Combined with the magnetic susceptibility and specific heat data, the thermal conductivity results point to a possible gapless QSL ground state of $\text{CeTa}_7\text{O}_{19}$.

We can estimate the mean free path (l_s) of the spinon excitations by using the formula [7]

$$\frac{\kappa_0}{T} = \frac{1}{3} \frac{C_s}{T} v_s l_s = \frac{\pi k_B^2}{9\hbar} \frac{l_s}{ad}. \quad (2)$$

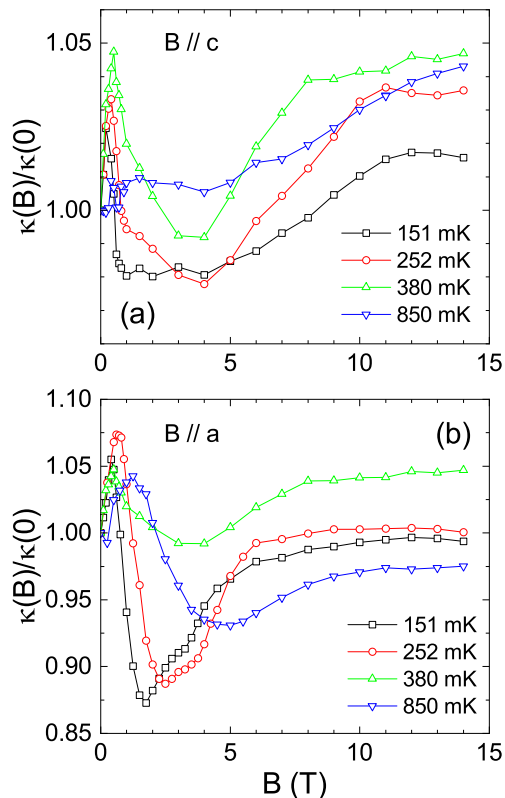


FIG. 6. Magnetic field dependence of thermal conductivity of the CeTa₇O₁₉ single crystal at different temperatures.

Here, C_s , v_s and l_s are the specific heat, velocity and mean free path of spinons, respectively, and C_s is assumed to have a linear temperature dependence. The a (~ 6.2371 Å) and d (~ 9.9915 Å) are nearest-neighbor intralayer and interlayer Ce-Ce distance, respectively. The spin exchange J is about 0.5 K, referring to the Curie-Weiss temperature. From the observed $\kappa_0/T = 0.0056$ W/K²m, the l_s is obtained as 110.8 Å, indicating that the excitations are mobile to a distance 18 times as long as the inter-spin distance without being scattered. In addition, the spinon specific heat is about $C_s = 4.80T$ J/mol K, which is much smaller than the Schottky term and is difficult to be separated from the experimental data.

Figure 6 shows the magnetic field dependence of thermal conductivity at different temperatures. In general, the magnetic field changes the κ rather weakly and the $\kappa(B)$ behaves similarly for different field directions. There are two features in these curves: a small peak and a broad valley at low fields and intermediate fields, respec-

tively. It is known that the sharp peak or sharp minimum on $\kappa(B)$ curves are usually associated with the magnetic transitions, as observed in many quantum magnetic materials [26, 27, 29, 46, 49, 50]. However, the magnetization data does not indicate any field-induced transition in CeTa₇O₁₉. Therefore, it is more likely that this low-field small peak is due to two competitive effects by the magnetic field. On one hand, the external field suppresses the spinon transport; on the other hand, it weakens the scattering between spinon and phonon. Whereas, the broad valley at $\kappa(B)$ reminds us the phonon resonant scattering by free spins [47, 51–53].

IV. SUMMARY

We grew high-quality CeTa₇O₁₉ single crystals and studied the low-temperature magnetic susceptibility, specific heat and thermal conductivity. The dc magnetic susceptibility and magnetization confirm that it is an effective spin-1/2 system with easy-axis anisotropy and antiferromagnetic spin coupling. The ultralow-temperature ac susceptibility and specific heat data indicate the absence of any phase transition down to 20 mK. The ultralow-temperature thermal conductivity at zero magnetic field exhibits a non-zero residual term $\kappa_0/T = 0.0056$ W/K²m, while the 14 T thermal conductivity shows an essential zero residual term. All these results suggest a possible ground state of quantum spin liquid.

ACKNOWLEDGMENTS

This work was supported by the National Key Research and Development Program of China (Grant No. 2023YFA1406500), the National Natural Science Foundation of China (Grants No. 12404043, No. 12274388, No. 12474098, No. 12104011, and No. 12204004) and the Nature Science Foundation of Anhui Province (Grant No. 2408085QA024). The work at the University of Tennessee was supported by the NSF with Grant No. NSF-DMR-2003117. H.W. and W.X. are supported by the U.S. DOE-BES under Contract No. DE-SC0023648. A portion of this work was performed at the National High Magnetic Field Laboratory, which is supported by National Science Foundation Cooperative Agreement No. DMR-2128556* and the State of Florida and the U.S. Department of Energy. M. L. and S. Z. acknowledge support from the LDRD program at Los Alamos National Laboratory.

- [1] L. Balents, Spin liquids in frustrated magnets, *Nature* (London) **464**, 199 (2010).
 [2] L. Savary and L. Balents, Quantum spin liquids: a review, *Rep. Prog. Phys.* **80**, 016502 (2016).

- [3] Y. Zhou, K. Kanoda, and T.-K. Ng, Quantum spin liquid states, *Rev. Mod. Phys.* **89**, 025003 (2017).
 [4] C. Broholm, R. Cava, S. Kivelson, D. Nocera, M. Norman, and T. Senthil, Quantum spin liquids, *Science* **367**,

- eaay0668 (2020).
- [5] P. W. Anderson, Resonating valence bonds: A new kind of insulator? *Mater. Res. Bull.* **8**, 153 (1973).
 - [6] B. Miksch, A. Pustogow, M. J. Rahim, A. A. Bardin, K. Kanoda, J. A. Schlueter, R. Hübner, M. Scheffler, and M. Dresse, Gapped magnetic ground state in quantum spin liquid candidate κ -(BEDT-TTF)₂Cu₂(CN)₃, *Science* **372**, 276 (2021).
 - [7] M. Yamashita, N. Nakata, Y. Senshu, M. Nagata, H. M. Yamamoto, R. Kato, T. Shibauchi, and Y. Matsuda, Highly mobile gapless excitations in a two-dimensional candidate quantum spin liquid, *Science* **328**, 1246 (2010).
 - [8] Y. Li, H. Liao, Z. Zhang, S. Li, F. Jin, L. Ling, L. Zhang, Y. Zou, L. Pi, Z. Yang, J. Wang, Z. Wu, and Q. Zhang, Gapless quantum spin liquid ground state in the two-dimensional spin-1/2 triangular antiferromagnet YbMgGaO₄, *Sci. Rep.* **5**, 16419 (2015).
 - [9] W. Liu, Z. Zhang, J. Ji, Y. Liu, J. Li, X. Wang, H. Lei, G. Chen, and Q. Zhang, Rare-earth chalcogenides: A large family of triangular lattice spin liquid candidates, *Chin. Phys. Lett.* **35**, 117501 (2018).
 - [10] R. Zhang, S. Guo, G. Xu, Z. Xu, and R. J. Cava, Strong quantum fluctuations in a quantum spin liquid candidate with a Co-based triangular lattice, *Proc. Natl. Acad. Sci. USA* **116**, 14505 (2019).
 - [11] M. Ashtar, Y. X. Gao, C. L. Wang, Y. Qiu, W. Tong, Y. M. Zou, X. W. Zhang, M. A. Marwat, S. L. Yuan, and Z. M. Tian, Synthesis, structure and magnetic properties of rare-earth REMgAl₁₁O₁₉ (RE = Pr, Nd) compounds with two-dimensional triangular lattice, *J. Alloys Compd.* **802**, 146 (2019).
 - [12] M. Ashtar, M. A. Marwat, Y. X. Gao, Z. T. Zhang, L. Pi, S. L. Yuan, and Z. M. Tian, REZnAl₁₁O₁₉ (RE = Pr, Nd, Sm–Tb): a new family of ideal 2D triangular lattice frustrated magnets, *J. Mater. Chem. C* **7**, 10073 (2019).
 - [13] F. Song, A. Liu, Q. Chen, J. Zhou, J. Li, W. Tong, S. Wang, Y. Wang, H. Lu, S. Yuan, H. Guo, and Z. Tian, Ba₆RE₂Ti₄O₁₇ (RE = Nd, Sm, Gd, Dy–Yb): A family of quasi-two-dimensional triangular lattice magnets, *arXiv:2311.08937* (2023).
 - [14] R. Bag, S. Xu, N. E. Sherman, L. Yadav, A. I. Kolesnikov, A. A. Podlesnyak, E. S. Choi, I. da Silva, J. E. Moore, and S. Haravifard, Evidence of Dirac Quantum Spin Liquid in YbZn₂GaO₅, *Phys. Rev. Lett.* **133**, 266703 (2024).
 - [15] B. R. Ortiz, P. M. Sarte, A. H. Avidor, A. Hay, E. Kenney, A. I. Kolesnikov, D. M. Pajerowski, A. A. Aczel, K. M. Taddei, C. M. Brown, C. Wang, M. J. Graf, R. Seshadri, L. Balents, and S. D. Wilson, Quantum disordered ground state in the triangular-lattice magnet NaRuO₂, *Nat. Phys.* **19**, 943 (2023).
 - [16] L. Clark, G. Sala, D. D. Maharaj, M. B. Stone, K. S. Knight, M. T. F. Telling, X. Wang, X. Xu, J. Kim, Y. Li, S.-W. Cheong, and B. D. Gaulin, Two-dimensional spin liquid behaviour in the triangular-honeycomb antiferromagnet TbInO₃, *Nat. Phys.* **15**, 262 (2019).
 - [17] Y. Shen, Y.-D. Li, H. Wo, Y. Li, S. Shen, B. Pan, Q. Wang, H. C. Walker, P. Steffens, M. Boehm, Y. Hao, D. L. Quintero-Castro, L. W. Harriger, M. D. Frontzek, L. Hao, S. Meng, Q. Zhang, G. Chen, and J. Zhao, Evidence for a spinon Fermi surface in a triangular-lattice quantum-spin-liquid candidate, *Nature* **540**, 559 (2016).
 - [18] Y. Li, D. Adroja, P. K. Biswas, P. J. Baker, Q. Zhang, J. Liu, A. A. Tsirlin, P. Gegenwart, and Q. Zhang, Muon Spin Relaxation Evidence for the U(1) Quantum Spin-Liquid Ground State in the Triangular Antiferromagnet YbMgGaO₄, *Phys. Rev. Lett.* **117**, 097201 (2016).
 - [19] Z. Zhu, P. A. Maksimov, S. R. White, and A. L. Chernyshev, Disorder-Induced Mimicry of a Spin Liquid in YbMgGaO₄, *Phys. Rev. Lett.* **119**, 157201 (2017).
 - [20] T. Arh, B. Sana, M. Pregelj, P. Khuntia, Z. Jagličić, M. D. Le, P. K. Biswas, P. Manuel, L. Mangin-Thro, A. Ozarowski and A. Zorko, The Ising triangular-lattice antiferromagnet neodymium heptatantalate as a quantum spin liquid candidate, *Nat. Mater.* **21**, 416 (2022).
 - [21] L. Wang, Z. Ouyang, T. Xiao, Z. Li, and Z. Tian, Synthesis, structure and magnetism of RTa₇O₁₉ (R = Pr, Sm, Eu, Gd, Dy, Ho) with perfect triangular lattice, *J. Alloys and Compd.* **937**, 168390 (2023).
 - [22] F. Pan, S. Sun, A. I. Kolesnikov, M. B. Stone, J. Huang, D. Xu, C. Shang, B. Shi, X. Gui, Z. Sun, J. Wang, J. Liu, H. Zhang, Z. Liu, and P. Cheng, Structural and magnetic characterization of CeTa₇O₁₉ and YbTa₇O₁₉ with two-dimensional pseudospin-1/2 triangular lattice, *Phys. Rev. B* **110**, 174448 (2024).
 - [23] J. A. M. Paddison, M. Daum, Z. Dun, G. Ehlers, Y. Liu, M. B. Stone, H. Zhou, and M. Mourigal, Continuous excitations of the triangular-lattice quantum spin-liquid YbMgGaO₄, *Nat. Phys.* **13**, 117 (2017).
 - [24] S. Yamashita, Y. Nakazawa, M. Oguni, Y. Oshima, H. Nojiri, Y. Shimizu, K. Miyagawa, and K. Kanoda, Thermodynamic properties of a spin-1/2 spin-liquid state in a κ -type organic salt. *Nat. Phys.* **4**, 459 (2008).
 - [25] S.-S. Lee and P. A. Lee, U(1) gauge theory of the Hubbard model: Spin liquid states and possible application to κ -(BEDT-TTF)₂Cu₂(CN)₃. *Phys. Rev. Lett.* **95**, 036403 (2005).
 - [26] X. Rao, G. Hussain, Q. Huang, W. J. Chu, N. Li, X. Zhao, Z. Dun, E. S. Choi, T. Asaba, L. Chen, L. Li, X. Y. Yue, N. N. Wang, J.-G. Cheng, Y. H. Gao, Y. Shen, J. Zhao, G. Chen, H. D. Zhou, and X. F. Sun, Survival of itinerant excitations and quantum spin state transitions in YbMgGaO₄ with chemical disorder, *Nat. Commun.* **12**, 4949 (2021).
 - [27] N. Li, Q. Huang, X. Y. Yue, W. J. Chu, Q. Chen, E. S. Choi, X. Zhao, H. D. Zhou, and X. F. Sun, Possible itinerant excitations and quantum spin state transitions in the effective spin-1/2 triangular-lattice antiferromagnet Na₂BaCo(PO₄)₂, *Nat. Commun.* **11**, 4216 (2020).
 - [28] H. Murayama, Y. Sato, T. Taniguchi, R. Kurihara, X. Z. Xing, W. Huang, S. Kasahara, Y. Kasahara, I. Kimchi, M. Yoshida, Y. Iwasa, Y. Mizukami, T. Shibauchi, M. Konczykowski, and Y. Matsuda, Effect of quenched disorder on the quantum spin liquid state of the triangular-lattice antiferromagnet 1T-TaS₂, *Phys. Rev. Research* **2**, 013099 (2020).
 - [29] S. Guang, N. Li, R. L. Luo, Q. Huang, Y. Wang, X. Yue, K. Xia, Q. Li, X. Zhao, G. Chen, H. Zhou, and X. Sun, Thermal transport of fractionalized antiferromagnetic and field-induced states in the Kitaev material Na₂Co₂TeO₆, *Phys. Rev. B* **107**, 184423 (2023).
 - [30] N. Li, M. T. Xie, Q. Huang, Z. W. Zhuo, Z. Zhang, E. S. Choi, Y. Y. Wang, H. Liang, Y. Sun, D. D. Wu, Q. J. Li, H. D. Zhou, G. Chen, X. Zhao, Q. M. Zhang, and X. F. Sun, Thermodynamics and heat transport of quantum spin liquid candidates NaYbS₂ and NaYbSe₂, *Phys. Rev. B* **110**, 224414 (2024).

- [31] A. Tari, *Specific Heat of Matter at Low Temperatures* (Imperial College Press, 2003).
- [32] B. Gao, T. Chen, D. W. Tam, C.-L. Huang, K. Sasmal, D. T. Adroja, F. Ye, H. Cao, G. Sala, M. B. Stone, C. Baines, J. A. T. Verezhak, H. Hu, J.-H. Chung, X. Xu, S.-W. Cheong, M. Nallaiyan, S. Spagna, M. B. Maple, A. H. Nevidomskyy, E. Morosan, G. Chen, and P. Dai, Experimental signatures of a three-dimensional quantum spin liquid in effective spin-1/2 $\text{Ce}_2\text{Zr}_2\text{O}_7$ pyrochlore, *Nat. Phys.* **15**, 1052 (2019).
- [33] R. Sibille, N. Gauthier, E. Lhotel, V. Porée, V. Pomjakushin, R. A. Ewings, T. G. Perring, J. Ollivier, A. Wildes, C. Ritter, T. C. Hansen, D. A. Keen, G. J. Nilsen, L. Keller, S. Petit, and T. Fennell, A quantum liquid of magnetic octupoles on the pyrochlore lattice, *Nat. Phys.* **16**, 546 (2020).
- [34] B. Gao, T. Chen, H. Yan, C. Duan, C.-L. Huang, X. P. Yao, F. Ye, C. Balz, J. R. Stewart, K. Nakajima, S. Ohira-Kawamura, G. Xu, X. Xu, S.-W. Cheong, E. Morosan, A. H. Nevidomskyy, G. Chen, and P. Dai, Magnetic field effects in an octupolar quantum spin liquid candidate, *Phys. Rev. B* **106**, 094425 (2022).
- [35] B. Gao, T. Chen, C. Liu, M. L. Klemm, S. Zhang, Z. Ma, X. Xu, C. Won, G. T. McCandless, N. Murai, S. Ohira-Kawamura, S. J. Moxim, J. T. Ryan, X. Huang, X. Wang, J. Y. Chan, S.-W. Cheong, O. Tchernyshyov, L. Balents, and P. Dai, Spin Excitation Continuum in the Exactly Solvable Triangular-Lattice Spin Liquid $\text{CeMgAl}_{11}\text{O}_{19}$, arXiv:2408.15957 (2024).
- [36] Z.-F. Ding, Y.-X. Yang, J. Zhang, C. Tan, Z.-H. Zhu, G. Chen, and L. Shu, Possible gapless spin liquid in the rare-earth kagome lattice magnet $\text{Tm}_3\text{Sb}_3\text{Zn}_2\text{O}_{14}$, *Phys. Rev. B* **98**, 174404 (2018).
- [37] J. Kim, X. Wang, F.-T. Huang, Y. Wang, X. Fang, X. Luo, Y. Li, M. Wu, S. Mori, D. Kwok, E. D. Mun, V. S. Zapf, and S.-W. Cheong, Spin Liquid State and Topological Structural Defects in Hexagonal TbInO_3 , *Phys. Rev. X* **9**, 031005 (2019).
- [38] H. Murayama, T. Tominaga, T. Asaba, A. de O. Silva, Y. Sato, H. Suzuki, Y. Ukai, S. Suetsugu, Y. Kasahara, R. Okuma, I. Kimchi, and Y. Matsuda, Universal scaling of specific heat in the $S = 1/2$ quantum kagome antiferromagnet herbertsmithite, *Phys. Rev. B* **106**, 174406 (2022).
- [39] B. Sana, M. Barik, M. Pregelj, U. Jena, M. Baenitz, J. Sichelschmidt, K. Sethupathi, P. Khuntia, Magnetic properties of a spin-orbit entangled $J_{eff} = 1/2$ three-dimensional frustrated rare-earth hyperkagome, arXiv:2304.07350 (2023).
- [40] R. Kumar, K. Nam, S.-H. Kim, K. H. Kim, and A. Sundaresan, Exploring potential quantum spin liquid state in a quasi-one-dimensional magnetic chain, *Phys. Rev. B* **109**, 224429 (2024).
- [41] C. Y. Jiang, B. L. Chen, K. W. Chen, J. C. Jiao, Y. Wang, Q. Wu, N. Y. Zhang, M. Y. Zou, P.-C. Ho, O. O. Bernal, and L. Shu, Persistent Spin Dynamics in the Ising Triangular-lattice Antiferromagnet $\text{Ba}_6\text{Nd}_2\text{Ti}_4\text{O}_{17}$, arXiv:2411.13070 (2024).
- [42] J. M. Ni, B. L. Pan, B. Q. Song, Y. Y. Huang, J. Y. Zeng, Y. J. Yu, E. J. Cheng, L. S. Wang, D. Z. Dai, R. Kato, and S. Y. Li, Absence of Magnetic Thermal Conductivity in the Quantum Spin Liquid Candidate $\text{EtMe}_3\text{Sb}[\text{Pd}(\text{dmit})_2]_2$, *Phys. Rev. Lett.* **123**, 247204 (2019).
- [43] Y. Xu, J. Zhang, Y. S. Li, Y. J. Yu, X. C. Hong, Q. M. Zhang, and S. Y. Li, Absence of Magnetic Thermal Conductivity in the Quantum Spin-Liquid Candidate YbMgGaO_4 , *Phys. Rev. Lett.* **117**, 267202 (2016).
- [44] Y. J. Yu, Y. Xu, L. P. He, M. Kratochvilova, Y. Y. Huang, J. M. Ni, L. Wang, S.-W. Cheong, J.-G. Park, and S. Y. Li, Heat transport study of the spin liquid candidate $1T\text{-TaS}_2$, *Phys. Rev. B* **96**, 081111(R) (2017).
- [45] N. Li, X. Zhao, and X.-F. Sun, Ultralow-Temperature Heat Transport in Quantum Spin Liquid Candidates: A Brief Review, *Chin. Phys. Lett.* **41**, 127501 (2024).
- [46] N. Li, Q. Huang, A. Brassington, X. Y. Yue, W. J. Chu, S. K. Guang, X. H. Zhou, P. Gao, E. X. Feng, H. B. Cao, E. S. Choi, Y. Sun, Q. J. Li, X. Zhao, H. D. Zhou, and X. F. Sun, Quantum spin state transitions in the spin-1 equilateral triangular lattice antiferromagnet $\text{Na}_2\text{BaNi}(\text{PO}_4)_2$, *Phys. Rev. B* **104**, 104403 (2021).
- [47] R. Berman, *Thermal Conduction in Solids* (Oxford University Press, Oxford, 1976).
- [48] X. F. Sun and Y. Ando, Comment on “Low-temperature phonon thermal conductivity of single-crystalline Nd_2CuO_4 : Effects of sample size and surface roughness”, *Phys. Rev. B* **79**, 176501 (2009).
- [49] X. F. Sun, W. Tao, X. M. Wang, and C. Fan, Low-Temperature Heat Transport in the Low-Dimensional Quantum Magnet $\text{NiCl}_2\text{-}4\text{SC}(\text{NH}_2)_2$, *Phys. Rev. Lett.* **102**, 167202 (2009).
- [50] Z. Y. Zhao, B. Tong, X. Zhao, L. M. Chen, J. Shi, F. B. Zhang, J. D. Song, S. J. Li, J. C. Wu, H. S. Xu, X. G. Liu, and X. F. Sun, Thermal conductivity of IPA-CuCl_3 : Evidence for ballistic magnon transport and the limited applicability of the Bose-Einstein condensation model, *Phys. Rev. B* **91**, 134420 (2015).
- [51] Q. J. Li, Z. Y. Zhao, H. D. Zhou, W. P. Ke, X. M. Wang, C. Fan, X. G. Liu, L. M. Chen, X. Zhao, and X. F. Sun, Paramagnetic ground state with field-induced partial order in $\text{Nd}_3\text{Ga}_5\text{SiO}_{14}$ probed by low-temperature heat transport, *Phys. Rev. B* **85**, 174438 (2012).
- [52] X. F. Sun, A. A. Taskin, X. Zhao, A. N. Lavrov, and Y. Ando, Large magnetothermal conductivity in $\text{GdBaCO}_2\text{O}_{5+x}$ single crystals, *Phys. Rev. B* **77**, 054436 (2008).
- [53] X. F. Sun, I. Tsukada, T. Suzuki, S. Komiya, and Y. Ando, Large magnetothermal effect and spin-phonon coupling in a parent insulating cuprate $\text{Pr}_{1.3}\text{La}_{0.7}\text{CuO}_4$, *Phys. Rev. B* **72**, 104501 (2005).